Near Surface Geophysics, 2013, **11**, 449-456 doi:10.3997/1873-0604.2013021

GPR investigations at an Inca-Spanish site in Argentina

Néstor Bonomo[1*], Ana Osella[1] and Norma Ratto[2]

[1] *Departamento de Física, Facultad de Ciencias Exactas y Naturales, Universidad de Buenos Aires – IFIBA, CONICET, Ciudad Universitaria, Buenos Aires 1428, Argentina*

[2] *Museo Etnográfico Juan B. Ambrosetti, Facultad de Filosofía y Letras, Universidad de Buenos Aires, Argentina*

Received September 2012, revision accepted February 2013

ABSTRACT

We present the results of a GPR prospecting carried out at the archaeological site of Batungasta, in the NW region of Argentina. This site was established by the Incas in the 14th century and was later occupied during the Spaniard conquest. Environmental information obtained at this arid zone led us to postulate that parts of the site buildings had been seriously damaged and buried by seasonal flood events as well as aeolian sedimentation. Therefore, we considered applying the GPR method to investigate the existence of buried remains, their architectural characteristics and to provide further evidence about the flows that possibly affected them. This method seemed suitable to attain these goals since it usually provides a good detection capacity for architectural structures and layers in dry environments, as well as good quality maps of the soil. Seven sectors of the site were surveyed using a GPR constant-offset methodology and 500 MHz antennas. The analysis of the data allowed recognizing electromagnetic patterns that could be associated to the existence of walls. In six of the seven sectors, enclosures formed by rock-earth and earth walls were detected and mapped, confirming Incaic-Spanish and Spanish structures, respectively. A sedimentary layer produced by a large flood that covered the structures was detected and mapped, providing evidence of this kind of event and its influence on the site. The maps of this layer were also useful to indirectly visualize the 3D shapes of the discovered walls, which were unclear in many sections of the data and to detect additional anthropogenic structures with very bad preservation conditions. These structures had not been previously identified from analysis of the data sections due to the confusing aspect of the reflections produced at their irregular boundaries.

INTRODUCTION

Geophysical methods

Geophysical methods such as Electromagnetic Induction (EMI), Electrical Resistivity Profiling (ERP), Seismics, Magnetometry and Ground Penetrating Radar (GPR) have been increasingly applied in the field of archaeology during the last two decades (Zananiri *et al*. 2010; Calia *et al*. 2012; Capizzi *et al*. 2012; Powell *et al*. 2012; Pérez-Gracia *et al*. 2012). An important reason for this success is that these methods allow detecting and mapping architectural structures with efficiency and without disturbing the soil, which is fundamental to protect these and other fragile objects from damage. In particular, GPR has become one of the most applied methods in archaeological prospecting because of its capabilities to explore large areas of soil in relatively short times and to produce very precise maps of foundations, walls, tunnels, vaults and also to detect smaller objects such as hearths and pottery (Masini *et al.* 2008; Rizzo *et al.* 2010; Bini *et al*. 2010; Bladon *et al*. 2011; Grangeia *et al*. 2011; Leucci *et al.* 2012; Porsani *et al*. 2012).

In the vast majority of applications performed in archaeology, GPR surveys are carried out by maintaining a constant distance between the emitting and receiving antennae (single-offset surveys, SO). A grid of equidistant parallel survey lines is commonly deployed in order to cover the entire area of study. The separation between the lines is typically about half a metre, which is sufficient to detect most kinds of architectural structures (e.g., Bonomo *et al*. 2012; Piro and Campana 2012). Denser grids are occasionally acquired to increase the spatial resolution in the cross-line direction, in cases in which it is important to obtain more details of the structures or to investigate smaller objects, such as detached pieces of masonry (Bonomo *et al.* 2010; Novo *et al.* 2012). Variable-offset acquisition, particularly, common-midpoint (CMP) acquisition, is sometimes performed at selected points of the investigated area to estimate a velocity for the electromagnetic waves propagating in the soil, from which the depths of the structures can be calculated. Although the CMP methodology can produce improved images of the subsoil (Yilmaz 1987), the acquisition and processing of these kind of data are much more time consuming than in the SO methodology, so that CMP surveys are normally limited to a few midpoints or survey lines (Berard and Maillol 2007; Brown *et al*. 2009).

* bonomo@df.uba.ar

Earth and composite rock-earth structures are the most frequent kinds of structures in the archaeological sites of the South Cone of America, so they are relevant targets for the GPR methodology. Due to the presence of raw-earth components, both kinds of structures are frail and become easily fragmented by natural or human factors. Uneven shapes of the resulting interfaces and spreading and mixing of the materials of the structures and the surrounding materials complicate the GPR reflections and their interpretation (Bonomo *et al*. 2010, 2012).

The Batungasta site

The archaeological site of Batungasta is located in the Andean region of the Catamarca Province of Argentina (27º52'47"S, 67º4'49"W). It operated as a pottery-manufacturing centre during the 14th century and was re-occupied at the time of the Spanish conquest, between the 15–16th centuries (Ratto *et al*. 2002). At present, only some segments of walls can be observed on the surface, with noticeable signs of deterioration. These walls consist of a lower part built with rocks and mud and an upper part built with raw-earth bricks (adobe). These characteristics have been considered as evidence of the Incaic Period and the subsequent Spanish occupation, respectively (Ratto *et al*. 2002). Segments of a wall fence constructed with rocks and mud, which surrounded an Inca Square, are also visible on the surface.

The shallowest portions of soil in Batungasta are composed of sandstone, gravel and mud deposits, overrun by aeolian sediments that form sparsely-distributed small dunes. Natural drainages and boulders are also visible on the surface. From the inspection of the archaeological remains of Batungasta and the alluvial fan of the nearby river La Troya, a series of contemporary environmental events that affected the zone were observed (Ratto *et al*. 2011). Two of these events showed noticeable intensities. The oldest of these events could be dated (700±60 BP) and was related to abundant silt-clay materials, which had a wide dispersion in the area and were located below the archaeological structures; the other was related to a large flow, which seemed to have dragged the boulders observed on the surface. This event occurred after the construction of the site, since many of the boulders were deposited on the wall remains.

Motivation and goals of this work

Considering the possible environmental history of Batungasta, the results of previous excavations carried out at the site and the lack of extensive knowledge about the site (Ratto 2005), we planned and carried out a GPR prospection of different sectors of the village to detect and map architectural structures that could have been buried by flood events and aeolian sedimentation. This was part of a larger archaeo-geophysical study, whose principal archaeological goal was obtaining evidence of sites in the region, most of them partially or totally deteriorated and buried by these kinds of processes, in order to better understand the characteristics of the consecutive occupations and their dynamics (Martino *et al*. 2005; Bonomo *et al.* 2010). In particular, Batungasta was one of the latest and most southern sites inhabited by the Incas in South America, with probably brief Inca and Spanish occupations, which makes it especially interesting for archaeologists. From a geophysical viewpoint, detecting buried walls in this site is interesting because hardly interpretable reflections were expected in the GPR images due to the probable very bad conservation conditions of the walls, as inferred from the remains observed on the surface. In general, architectural structures that suffered significant collapses tend to produce complex reflections as a consequence of the unevenness of the resulting interfaces and the superposition of reflections from the detached fragments around (e.g., Bonomo *et al.* 2010). In Batungasta, reflections at rocks dragged by floods and retained at the structures were also expected, which would contribute to the complex overall response. Moreover, the walls of this site have been partially constructed with raw-earth materials extracted from the surrounding soil. This usually produces moderate or low

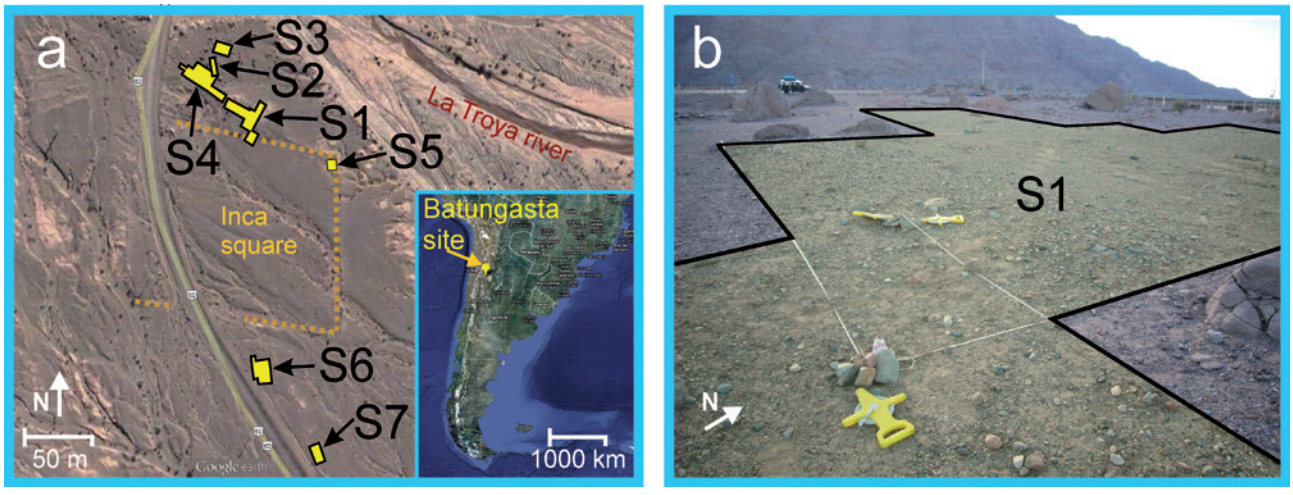

FIGURE 1

Batungasta archaeological site: (a) location of the prospected sectors (S1–S7), (b) picture of the site. The shadowed area corresponds to sector S1.

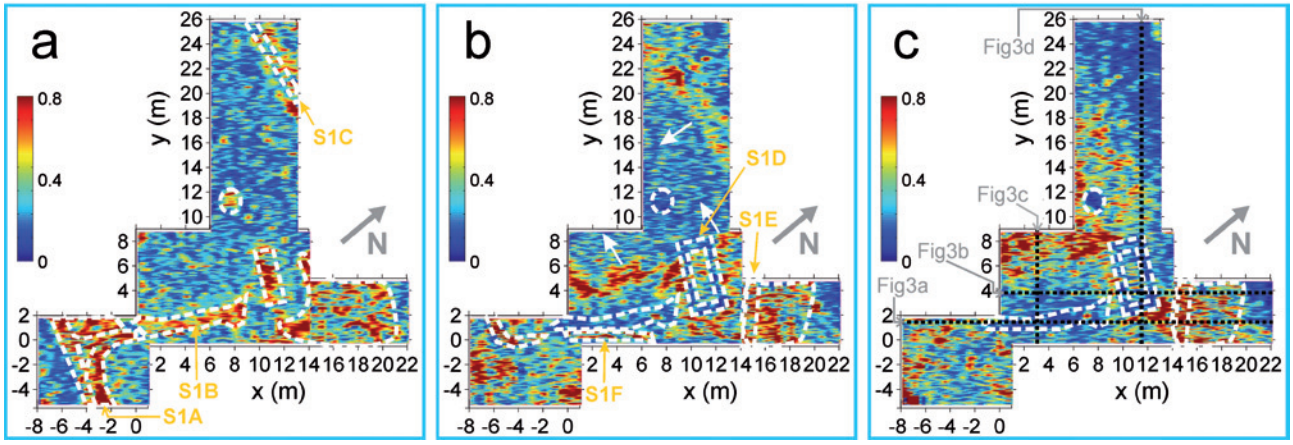

FIGURE 2

Constant-time slices of the intensity of the data acquired in S1, for two-way traveltimes (a) 3.1 ns, (b) 7.0 ns and (c) 10.9 ns. These times correspond to approximate depths of 20 cm, 45 cm and 70 cm, respectively. Relatively low- and high-intensity sub-areas have been delimited with dashed lines. Sub-areas with approximately linear shapes are indicated with labels S1A–S1F. The dotted lines in (c) correspond to the profiles shown in Fig. 3.

contrasts of the physical properties at the interfaces, especially, in cases of mixing of materials, which can lead to low-intensity reflections with respect to the background clutter and noise, thus further complicating the GPR images and their interpretation. In these cases, it could be necessary to sharpen the usual methodologies or develop alternative ones to properly identify the archaeological structures in the soil.

In the following section, we start the description of the GPR prospecting carried out in Batungasta by explaining the applied methodology. Then, representative vertical and constant-time slices of the data are shown and analysed. We initially focus on possible signals of architectural structures. Then, the images are analysed in order to obtain information about possible floods that could affect the site. Maps of sedimentary layers probably produced by this kind of flow, obtained from the GPR data, are shown. These maps are used to indirectly visualize the 3D shapes of the structures below them, including possible archaeological structures not visible in the vertical and time slices of the data. The overall interpretations of the structures detected in the soil and the results of the excavations performed to check them are described. Concluding remarks are finally given in the last section of the work.

METHODOLOGY

The studied area consisted in seven sectors with almost flat topographies (S1–S7 in Fig. 1a), which covered a total area of 812 m^2. The sectors were selected near visible archaeological structures, in order to investigate their continuity. Their shapes were limited by these structures, as well as natural drainages and large outcropping boulders. We used a Sensors & Software Pulse EKKO PRO radar unit, with 500 MHz antennas, since this frequency usually provides good resolution and penetration for archaeological structures such as walls and foundations. The surveys were conducted with a constant-offset methodology (offset = 25 cm). Each sector was covered with two orthogonal grids of parallel lines, deployed along the x and y directions, respectively, with cross-line spacing of 0.5 m and in-line sampling intervals of 0.025 m. This assured enough sampling density in both directions for these kinds of targets. The stacking of traces was 16. To process and visualize the data we used software developed by our research group on a Matlab platform (Bonomo *et al.* 2010, 2012). The general processing flow for the data was the following: time-zero correction, dewow filtering, background subtraction, broadband pass filtering in space and time and application of gain.

The data were interpreted by representing their amplitudes and intensities in vertical sections and constant-time slices. In the case of the intensity images, the absolute value of the amplitude of the data was averaged in time through a one-period interval before representing it. Hyperbola fitting was performed on the diffraction signals observed in the vertical sections to estimate mean propagation velocities. We averaged these values to obtain v = (12.8 +/-0.9) cm/ns, which was used to convert times to depths.

RESULTS

In the next paragraphs, we focus on the results of sectors S1–S3 to explain the main characteristics of the data and their interpretation. We then show the overall results for S1–S4 and S5–S7 and the main results of the test excavations.

Sector S1

Sector S1 (Fig. 1) occupied an area of 348 m^2, located close to the Inca square. The NE border of the sector was surrounded by a natural channel, the NW and E borders by remains of walls, whereas several boulders were spread along the rest of the perimeter. To simplify the acquisition of the data, the sector was divided into four rectangular sub-sectors (not marked in Fig. 1). A total of 80 x-profiles and 80 y-profiles were acquired.

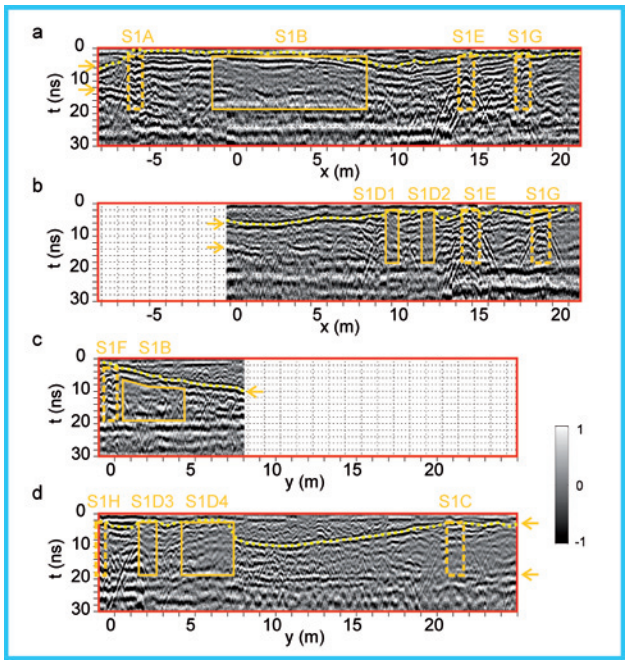

FIGURE 3
Vertical sections of the data acquired in S1 for (a) y = 1.5 m, (b) y = 4.0 m, (c) x = 3.0 m and (d) x = 11.5 m. The small arrows indicate a number of quasi-horizontal reflections, whereas the dashed and full lines indicate anomalous areas showing groups of diffraction signals or low- intensity amplitudes, respectively. We used the same labelling as in Fig. 2. The dotted lines indicate a prominent reflection that extends over the entire sector.

Figure 2 shows constant-time slices of the intensity of the data acquired in S1, for two-way traveltimes 3.1 ns (Fig. 2a), 7.0 ns (Fig. 2b) and 10.9 ns (Fig. 2c), which correspond to approximate depths of 20 cm, 45 cm and 70 cm, respectively (v = (12.8 +/-0.9) cm/ns, as explained above). A number of relatively low- and high-intensity areas can be observed in the figures (dashed lines). Some of them present elongated shapes, as those labelled S1A– S1F. This characteristic is important in archaeological prospecting, since linear features can indicate buried architectural structures such as walls, foundations, borders of floors, etc.

Figure 3 shows vertical sections of the data acquired in S1, for y = 1.5 m (Fig. 3a), y = 4.0 m (Fig. 3b), x = 3.0 m (Fig. 3c) and x = 11.5 (Fig. 3d). The positions of these profiles in the sector have been indicated with dotted lines in the previous figure (Fig. 2c). A number of quasi-horizontal reflections are observed in Fig. 3. This pattern of reflections is altered at some areas by groups of diffraction hyperbolae or by areas with lower intensities, as those marked with dashed and full lines, respectively. We named these anomalies with the same labels as in Fig. 2. Note that S1D1, S1D2, S1D3 and S1D4 in Fig. 3(b) and Fig. 3(d) correspond to the four sides of the polygon S1D in Fig. 2(b), whereas the areas S1G and S1H are shown in Fig. 3 but not in Fig. 2.

Most of the anomalies in Fig. 3 have characteristics that resemble typical electromagnetic responses of walls (e.g., Bonomo *et al.* 2010). For example, anomalies S1A, S1C, S1D1, S1D2, S1D3, S1D4, S1E, S1F, S1G and S1H show reflections similar to those produced at the tops of these kind of structures and diffraction hyperbolae similar to those produced at their upper and lateral edges. The lines marked in the figures approximately agree with the positions of these reflectors. S1A, S1C, S1E, S1F, S1G and S1H also show diffractions inside the marked areas, probably due to rocks that are part of the structures. On the contrary, S1D1, S1D2, S1D3 and S1D4 do not present diffractions inside. The low-reflection amplitudes at their interior indicate a rather homogeneous composition of the respective structures, probably due to an earth wall. S1D4 is wider than the other anomalies since the associated survey line crosses one of the structures in a diagonal form, as observed in Fig. 2(c). In general, the detected structures showed widths between 0.6–0.8 m and heights below 1 m, which agree with the sizes of the walls observed on the surface (0.6–1.0 m). In relation to the low-intensity area S1B, it was interpreted

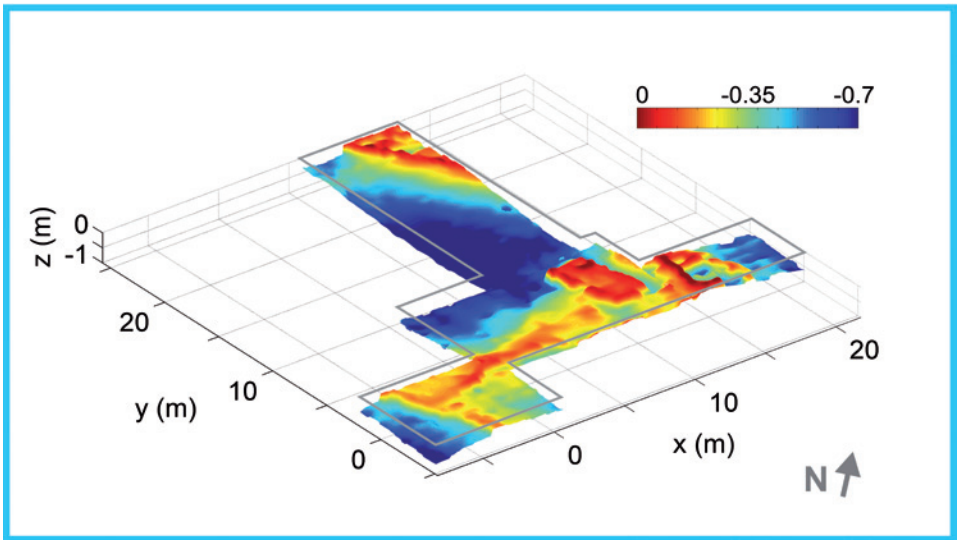

FIGURE 4
Map of the main reflector detected in S1. The colour scale is proportional to the depth scale. The shape of the walls below this reflector can be clearly distinguished in the figure.

as produced by earth collapsed from the structures S1F, e.g., adobe materials or mortar from the earth-rock wall.

A clear reflection produced at a smooth interface between two media can be observed in Fig. 3 (dotted lines). This reflection is produced at the top of a sedimentary layer that extends over the entire sector and that covers the detected walls. Figure 4 shows the shape of this reflector throughout S1. The surface was constructed by picking points in time-migrated sections of the data, as usually done to follow layers in geological and engineering applications (e.g., Donohue *et al*. 2011; Tye *et al*. 2011). We used the aforementioned velocity, v = (12.8 +/-0.9) cm/ns, to migrate the data and to convert times to depths. For a more simple visualization of the result, we made the colour scale of the figure proportional to the depth scale. We note that the reflector in the figure indirectly defines all the structures mentioned up to now with clarity. Also, different areas with collapsed materials can be observed around these structures.

From the analysis of the images obtained in S1, several structures similar to walls were detected, as well as other linear features with probable anthropological origin. A map of these anomalies and their main interpretations are shown in Fig. 5. In this figure, we also indicate the positions of the walls and boulders observed on the surface. As main results, the walls detected in S1 have completed a number of enclosures in the central and northern parts of the sector and have continued visible segments in its southern part.

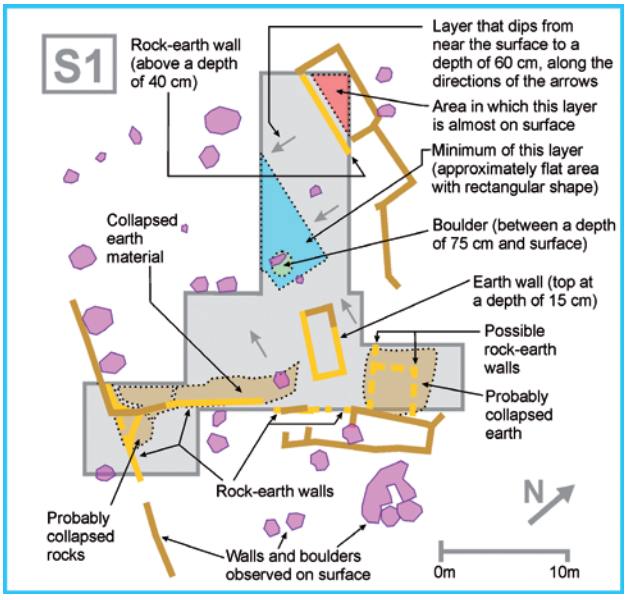

FIGURE 5
Schematic view of the main structures detected in sector S1 and their corresponding interpretations.

Sector S2

S2 occupied a rectangular area of 4 m x 13 m, surrounded by boulders. We acquired a total of 9 x-profiles and 27 y-profiles. The time slices of S2 did not present clear anomalous areas but the vertical sections showed a number of reflections that could be associated to characteristic signals of rock-earth walls. Figure 6(a) shows one of these sections (x = 2.125 m). The positions of the probable wall responses are indicated with dashed lines in the figure. We also indicate a clear reflection produced at a smooth interface (dotted line), supposedly the same as detected and mapped in sector S1. Figure 6(b) is a map of this reflector. We observe that the surface in the figure clearly delineates a number of walls that constitute a rectangular enclosure. Probable collapses of materials from the walls can be observed near the NE and SE vertices of the enclosure. Collapses would explain why anomaly S2A is wider than S2B and the other anomalies shown in S1 (Fig. 3). Also, a small opening can be observed near the NE vertex of the enclosure.

Sector S3

This sector consisted in a rectangular area of 8 m x 14 m, which was bounded by boulders. As in sector S2, the time slices of S3 did not present clear anomalies. Figure 7(a) shows vertical sections of the sector (x = 1.625 m, x = 5.625 m, y = 4.875 m, y = 10.875 m). The characteristic signals of a rocky wall can be observed near the SW corner of S3 (anomaly S3A, rectangle with dashed lines). Also, some areas with relatively low-intensity signals and apparently related to more homogeneous sediments appear in different parts of the sector (anomalies S3B, rectangles with dotted lines). As in the previous sectors, evident reflections at a smooth interface can be observed in S3 (dotted curves). Figure 7(b) shows a map of this reflector extending through the sector. The surface in the figure delineates two structures similar to walls around the position of S3, which form an angle of approximately 90 degrees. On the contrary, S3B is very irregular and did not show clear signals of walls. In spite of this, S3B presents a bounded aspect and a global size compatible with the structures detected in S1 and S2, which suggest the possibility of deteriorated walls below.

OVERALL RESULTS

Similar anomalies to those described in the previous sections appear in other sectors of Batungasta. Figure 8(a) shows a picture of sectors S1–S4 and Fig. 8(b) a map of the anomalies found in them and their main interpretations. Figure 9(a,b) is an analogy of Fig. 8 but for sectors S5–S7. Buried walls were identified in all the sectors, except S5. Also a number of linear features that could not be clearly related to walls were detected in the vertical sections of the data. Finally, sedimentary layers that covered the archaeological structures, as those shown in Figs 4, 6 and 7, were detected through the site. To investigate their continuity, we acquired additional survey lines that connected all the prospected sectors and extended over other parts of the site. The analysis of these profiles indicated that all the layers actually correspond to a single one.

A series of localized excavations were carried out at different points to corroborate our interpretations of the GPR data (Fig. 10). Most of the predicted walls were checked in this manner. We verified that the S1D anomaly (Figs 2–5) corresponded to an earth wall (adobe) and that the other walls in sector S1 had

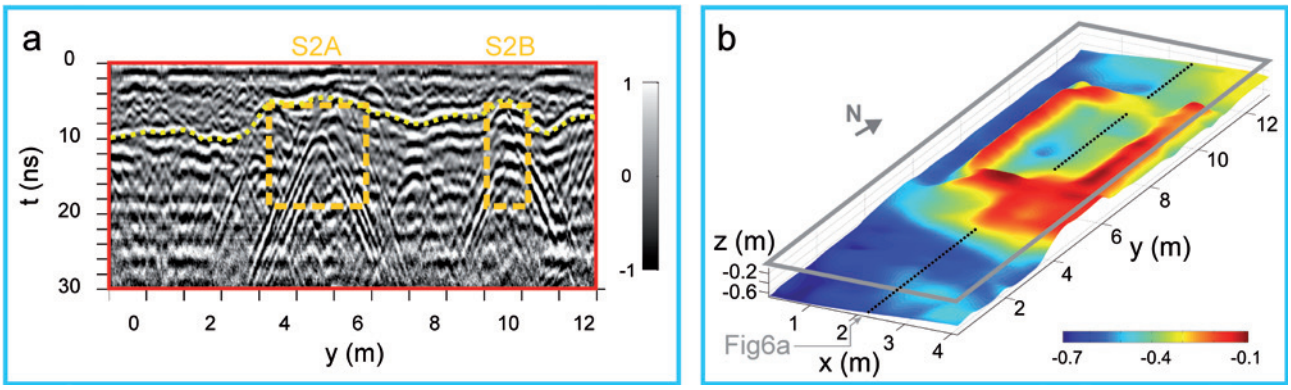

FIGURE 6

a) Vertical section of the data acquired in sector S2 (x = 2.125 m). Probable wall responses are indicated with dashed lines. The dotted line corresponds to a clear reflection produced at a smooth interface. b) Map of this interface (colour scale proportional to the depth scale). With a dotted line, we have indicated the position of the profile shown in a).

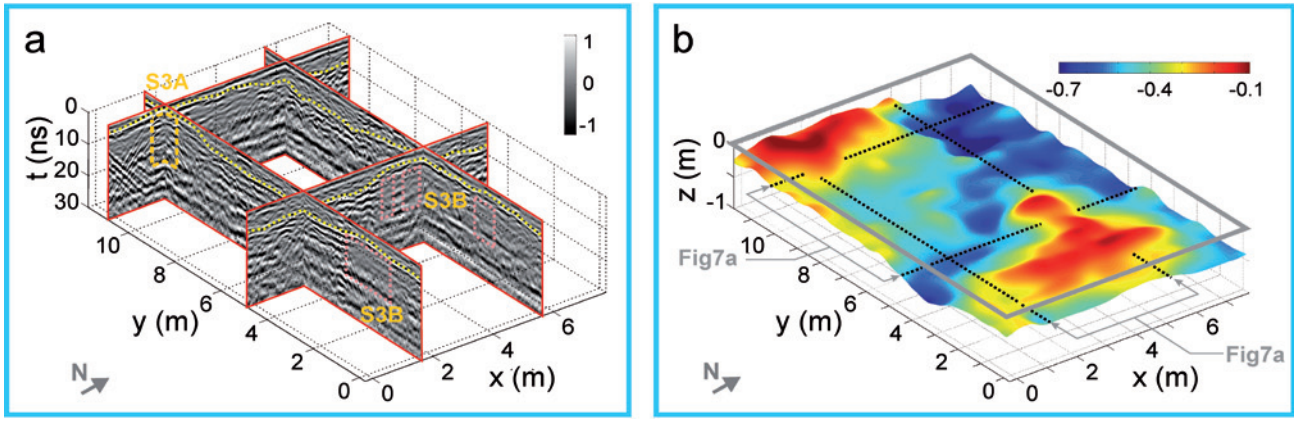

FIGURE 7

a) Vertical sections of the data acquired in sector S3. The positions of the respective profiles are x = 1.625 m, x = 5.625 m, y = 4.875 m and y = 10.875 m. A probable wall response is indicated with a dashed-line rectangle (anomaly S3A). Some relatively low-intensity areas are marked with dotted-line rectangles (anomalies S3B). Dotted curves indicate a noticeable reflection at a smooth interface. b) Map of this interface (colour scale proportional to the depth scale). With dotted lines, we have indicated the positions of the profiles shown in a).

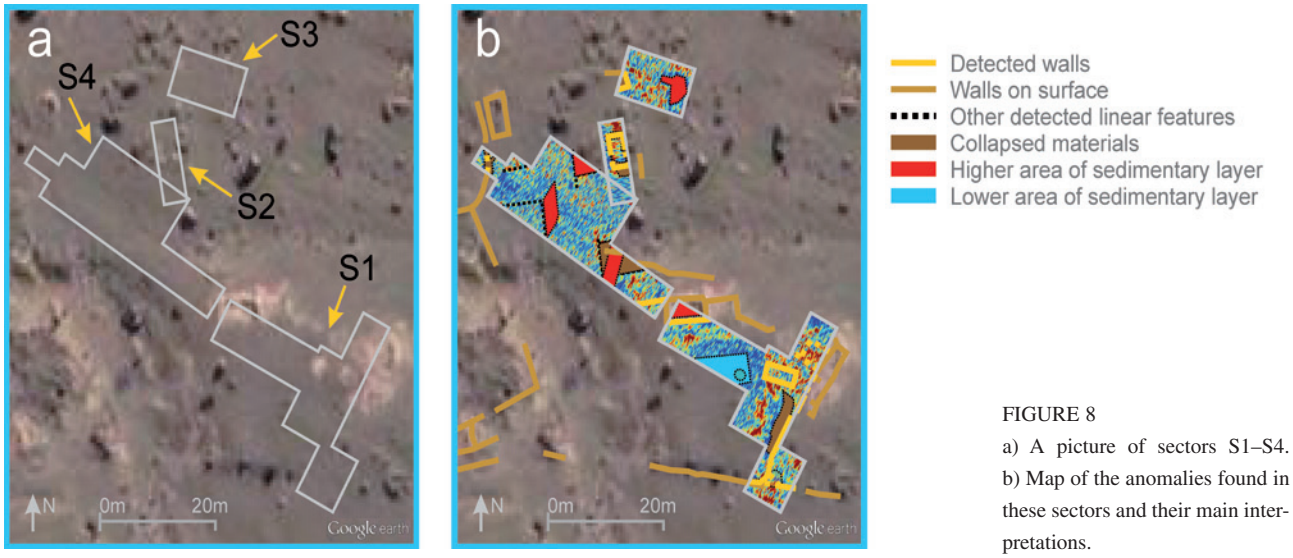

FIGURE 8

a) A picture of sectors S1–S4. b) Map of the anomalies found in these sectors and their main interpretations.

been constructed with rocks and earth (Fig. 10b,c, respectively). Bad conservation conditions and significant collapses of the structures were corroborated in most of the tests. In particular, rocks and earth collapsed from one of the walls of S2 could be corroborated in the area around anomaly S2D (Fig. 6).

In these excavations we also tested the layer that covered the archaeological structures, an alluvial layer mostly composed of gravel and silt. Mixing of the materials of this layer and the walls has been observed around the structures. The anthological origin of some of the structures below it, indirectly detected from the maps of the layer, was established. In particular, in the area of the anomalies S3B, we found abundant materials of a wall, as well as in S4 and S7.

CONCLUSIONS

The GPR prospecting carried out at the Batungasta archaeological site allowed detecting and characterizing several buried structures. Earth and rock-earth composite walls were detected in six of the seven prospected sectors, as well as other probable anthropogenic features. The analysis of the GPR images made possible to clearly distinguish between both kinds of walls, which are the most frequent in the archaeological sites of the region. The coexistence of these structures has provided evidence of the Inca and Spanish occupations of Batungasta, respectively. The discovered structures completed the layout observed on the surface by connecting different wall segments, projecting new segments in other directions and delimiting up-to-now

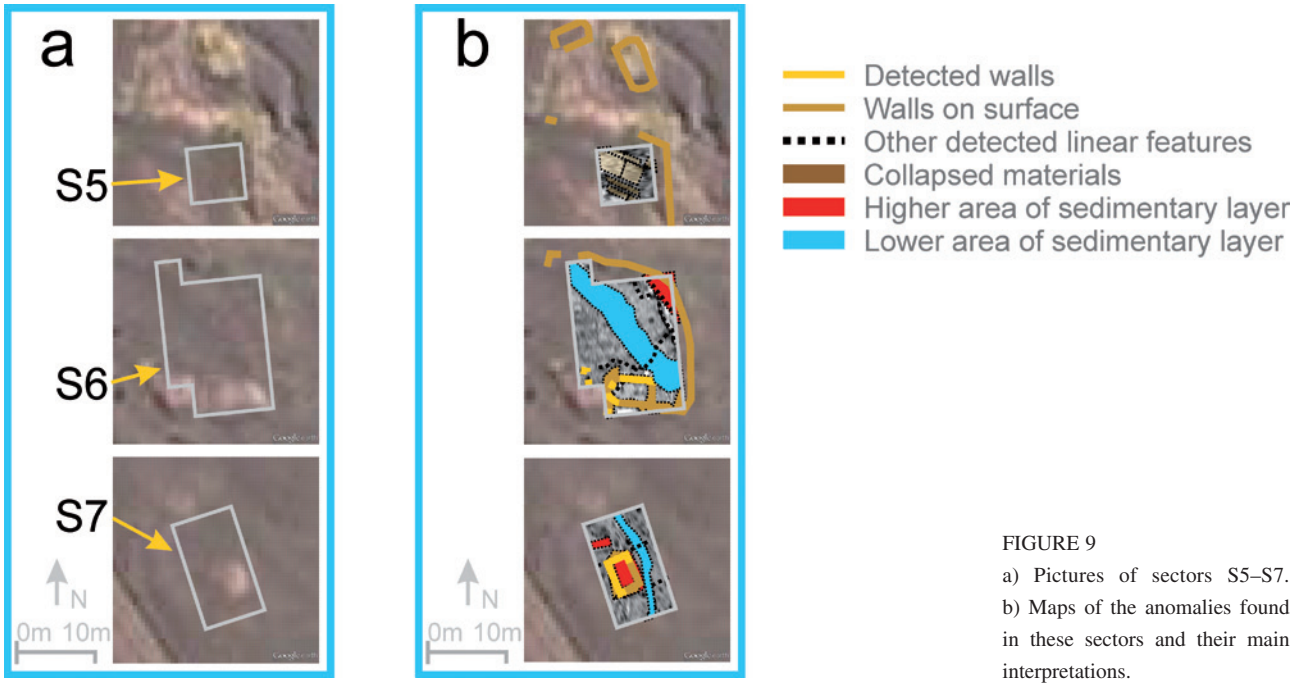

FIGURE 9
a) Pictures of sectors S5–S7. b) Maps of the anomalies found in these sectors and their main interpretations.

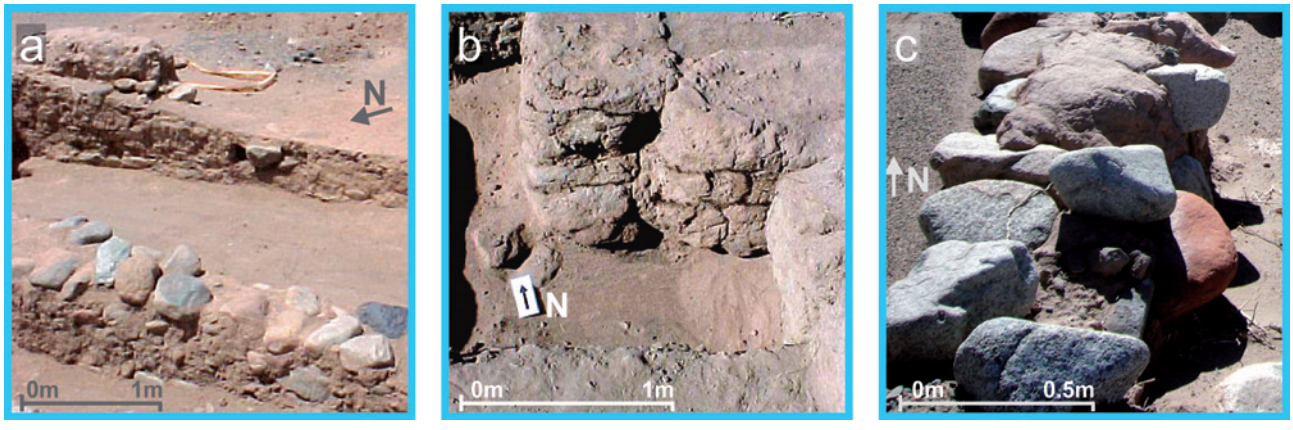

FIGURE 10
Test excavations performed at the Batungasta site. a) Two approximately parallel walls with a basis constructed with rocks and earth mortar. Remains of adobe material are visible on the wall located at the bottom (upper-left corner of the figure). b) Adobe wall. c) Closer view of a wall constructed with rocks and earth mortar.

unknown enclosures, which provide important information on the architectural characteristics of the site.

Evident reflections produced by a sedimentary layer that covered the archaeological structures were detected in the site. This layer seems to be related to one of the environmental events postulated in Batungasta, a large flood from the La Troya River that occurred after the construction of the site and that covered it. Soil analysis and radiocarbon dating are planned for the future to obtain more information about this event, in order to understand in more detail the environmental and population dynamics of the site.

GPR maps of this layer were constructed and used to visualize the 3D shapes of the detected walls. This could not be completely achieved by directly picking points along the reflections of the structures since significant collapses and mixing of materials made these reflections unclear along many segments of the walls. The maps also allowed detecting additional possibly anthropogenic structures, of which some were found to be the remains of earth walls. These structures had not been previously identified from analysis of the data sections due to the confusing aspect of the reflections produced at their very irregular boundaries. As a result, this methodology, which is rather frequent in geological and engineering applications, appears as potentially useful also in archaeological prospection, to obtain maps that complete or reinforce the information obtained from other sources, such as anomaly and texture maps.

ACKNOWLEDGEMENTS

This work was partially supported by PICT-2007-01539, UBACyT-F139 and CONICET (PIP 2009-00582).

REFERENCES

Berard B. and Maillol J. 2007. Multi-offset ground penetrating radar data for improved imaging in areas of lateral complexity – Application at a Native American site. *Journal of Applied Geophysics* **62**, 167–177.

Bini M., Fornaciari A., Ribolini A., Bianchi A., Sartini S. and Coschino F. 2010. Medieval phases of settlement at Benabbio castle, Apennine Mountains, Italy: Evidence from Ground Penetrating Radar survey. *Journal of Archaeological Science* **37**, 3059–3067.

Bladon P. Moffat I., Guilfoyle D., Beale A. and Milani J. 2011. Mapping anthropogenic fill with GPR for unmarked grave detection: A case study from a possible location of Mokare's grave, Albany, Western Australia. *Exploration Geophysics* **42**, 249–257.

Bonomo N., Osella A., Martinelli P., de la Vega M., Cocco G., Letieri F. and Frittegotto G. 2012. Location and characterization of the Sancti Spiritus Fort from geophysical investigations. *Journal of Applied Geophysics* **83**, 57–64.

Bonomo N., Osella A. and Ratto N. 2010. Detecting and mapping buried buildings with GPR at an ancient village in Northwestern Argentina. *Journal of Archaeological Science* **37**, 3247–3255.

Brown J., Nichols J., Steinbronn L. and Bradford J. 2009. Improved GPR interpretation through resolution of lateral velocity heterogeneity: Example from an archaeological site investigation. *Journal of Applied Geophysics* **68**, 3–8.

Calia A., Leucci G., Masini N., Matera L., Persico R. and Sileo M. 2012. Integrated prospecting in the crypt of the Basilica of Saint Nicholas in Bari, Italy. *Journal of Geophysics and Engineering* **9**, 271–281.

Capizzi P., Martorana R., Messina P. and Cosentino P. 2012. Geophysical and geotechnical investigations to support the restoration project of the Roman 'Villa del Casale', Piazza Armerina, Sicily, Italy. *Near Surface Geophysics* **10**, 145–160.

Donohue S., Gavin K. and Tolooiyan A. 2011. Geophysical and geotechnical assessment of a railway embankment failure. *Near Surface Geophysics* **9**, 33–44.

Grangeia C., Matias M., Figueiredo F., Hermozilha H., Carvalho P. and Silva R. 2011. A multi-method high-resolution geophysical survey in the Machado de Castro museum, central Portugal. *Journal of Geophysics and Engineering* **8**, 351–365.

Leucci G., Masini N., Persico R., Quarta G. and Dolce C. 2012. A multidisciplinary analysis of the Crypt of the Holy Spirit in Monopoli (southern Italy). *Near Surface Geophysics* **10**, 57–64.

Martino L., Bonomo N., Lascano E., Osella A. and Ratto N. 2006. Electrical and GPR prospecting at Palo Blanco archaelogical site, northwestern Argentina. *Geophysics* **71**(6), B193–B199.

Masini N., Rizzo E., Lasaponara R. and Orefici G. 2008. Integrated remote sensing techniques for the detection of buried archaeological adobe structures: Preliminary results in Cahuachi (Peru). *Advances in Geosciences* **19**, 75–82.

Novo A., Lorenzo H., Rial F. and Solla M. 2012. From pseudo-3D to full-resolution GPR imaging of a complex Roman site. *Near Surface Geophysics* **10**, 11–15.

Pérez-Gracia V., González-Drigo R. and Sala R. 2012. Ground-penetrating radar resolution in cultural heritage applications. *Near Surface Geophysics* **10**, 77–87.

Piro S. and Campana S. 2012. GPR investigation in different archaeological sites in Tuscany (Italy). Analysis and comparison of the obtained results. *Near Surface Geophysics* **10**, 47–56.

Porsani J., de Matos Jangelme G. and Kipnis R. 2012. Use of ground-penetrating radar to map subsurface features at the Lapa do Santo archaeological site (Brazil). *Near Surface Geophysics* **10**, 141–144.

Powell A., Wheeler J. and Batt C. 2012. Identifying archaeological wood stack charcoal production sites using geophysical prospection: Magnetic characteristics from a modern wood stack charcoal burn site. *Journal of Archaeological Science* **39**, 1197–1204.

Ratto N. 2005. La Arqueología del Bolsón de Fiambalá a través de los Estudios de Impacto (Dpto. Tinogasta, Catamarca, Argentina). Actas dos I Jornadas Internacionais Vestígios do Passado. AGIR - Associação para a Investigação e Desenvolvimento Sócio-cultural (972-99404-1-X). Lisboa.

Ratto N., Bonomo N., de La Vega M. and Osella A. 2011. Arqueogeofísica y paleoambiente en el oeste tinogasteño (Dpto. Tinogasta, Catamarca): Resultados preliminares. III Congreso Latinoamericano de Arqueometría, Arica, Chile. Expanded Abstracts, 88–89.

Ratto N., Orgaz M. and Plá R. 2002. Producción y distribución de bienes cerámicos durante la ocupación Inca entre la región puneña de Chaschuil y el valle de Abaucán (Dpto. Tinogasta, Catamarca). *Relaciones de la Sociedad Argentina de Antropología* **27**, 271–301.

Rizzo E., Masini N., Lasaponara R. and Orefici G. 2010. Archaeo-Geophysical methods in the Templo del Escalonado (Cahuachi, Nasca, Perù). *Near Surface Geophysics* **8**, 433–439.

Tye A., Kessler H., Ambrose K., Williams J., Tragheim D., Scheib A. *et al*. 2011. Using integrated near-surface geophysical surveys to aid mapping and interpretation of geology in an alluvial landscape within a 3D soil-geology framework. *Near Surface Geophysics* **9**, 15–31.

Yilmaz O. 1987. *Seismic Data Processing*. 4th edition. Society of Exploration Geophysicists. Tulsa, USA.

Zananiri I., Hademenos V. and Piteros C. 2010. Geophysical investigations near the ancient Agora at the city of Argos, Greece. *Journal of Geophysics and Engineering* **7**, 174–182.